

## 3D printed dental implants with a porous structure: The in vitro response of osteoblasts, fibroblasts, mesenchymal stem cells, and monocytes

Giovanna Iezzi<sup>a,†</sup>, Barbara Zavan<sup>b,†</sup>, Morena Petrini<sup>a</sup>, Letizia Ferroni<sup>c</sup>,  
Tania Vanessa Pierfelice<sup>a</sup>, Ugo D'Amora<sup>d</sup>, Alfredo Ronca<sup>d</sup>, Emira D'Amico<sup>a,\*</sup>, Carlo Mangano<sup>e</sup>

<sup>a</sup> Department of Medical, Oral and Biotechnological Sciences, University "G. d'Annunzio" Chieti-Pescara, Via dei Vestini, 31, Chieti 66100, Italy

<sup>b</sup> Translational Medicine Department, University of Ferrara, Ferrara 44121, Italy

<sup>c</sup> Maria Cecilia Hospital, GVM Care & Research, Cotignola, Ravenna 48033, Italy

<sup>d</sup> Institute of Polymers, Composites and Biomaterials National Research Council (IPCB-CNR), Naples 80125, Italy

<sup>e</sup> Private Practice, Gravedona, CO, Italy

### ARTICLE INFO

#### Keywords:

3D printed implant  
Selective laser melting  
Osteoblast  
Gingival fibroblasts  
Mesenchymal stem cells  
Monocytes

### ABSTRACT

**Aims:** The first aim of this study was to characterize the surface topography of a novel 3D-printed dental implant at the micro- and macro-level. Its second aim was to evaluate the osteogenic, angiogenic, and immunogenic responses of human oral osteoblasts (hOBs), gingival fibroblasts (hGFs), mesenchymal stem cells (hAD-MSCs), and monocytes to this novel implant surface.

**Methods:** A 3D-printed Ti-6Al-4 V implant was produced by selective laser melting and subjected to organic acid etching (TEST). It was then compared to a machined surface (CTRL). Its biological properties were evaluated via cell proliferation assays, morphological observations, gene expression analyses, mineralization assessments, and collagen quantifications.

**Results:** Scanning electron microscopy analysis showed that the TEST group was characterized by a highly interconnected porous architecture and a roughed surface. The morphological observations showed good adhesion of cells cultured on the TEST surface, with a significant increase in hOB growth. Similarly, the gene expression analysis showed significantly higher levels of osseointegration biomarkers. Picrosirius staining showed a slight increase in collagen production in the TEST group compared to the CTRL group. hAD-MSCs showed an increase in endothelial and osteogenic commitment-related markers. Monocytes showed increased mRNA synthesis related to the M2 (anti-inflammatory) macrophagic phenotype.

**Conclusions:** Considering the higher interaction with hOBs, hGFs, hAD-MSCs, and monocytes, the prepared 3D-printed implant could be used for future clinical applications.

**Clinical relevance:** This study demonstrated the excellent biological response of various cells to the porous surface of the novel 3D-printed implant.

### Acronym

ACTB  $\beta$ -actin  
ALCAM activated leukocyte cell adhesion molecule  
ALP alkaline phosphatase  
AM additive manufacturing  
BMP2 bone morphogenetic protein 2  
CAD computer-aided design  
CD44 cluster of differentiation 44

CO<sub>2</sub> carbon dioxide  
CPC cetylpyridinium chloride  
ECM extracellular matrix  
ENG endoglin  
FN1 fibronectin 1  
GAPDH glyceraldehyde-3-phosphate dehydrogenase  
hAD-MSCs human adipose mesenchymal stem cells  
hGFs human gingival fibroblasts  
hOBs human oral osteoblasts

\* Corresponding author.

E-mail address: [emira.damico@unich.it](mailto:emira.damico@unich.it) (E. D'Amico).

† The two first authors equally contributed to the manuscript.

ICAM	intercellular adhesion molecule 1
IGF1	insulin-like growth factor 1 (IGF1)
miRNAs	microRNAs
mRNA	messenger RNA
MTT	dimethyl thiazolyl diphenyl tetrazolium salt assay
OAE	organic acid etching
OCN	osteocalcin
OPN	osteopontin
PECAM1/CD31	platelet and endothelial cell adhesion molecule 1
RT-qPCR	real-time quantitative polymerase chain reactions
SDs	standard deviations
SEM	scanning electron microscope
SLM	selective laser melting
VEGFA	vascular endothelial growth factor A
VWF	von Willebrand factor

## 1. Introduction

The clinical success in implant dentistry depends on several biological and mechanical parameters [1]. The interaction between the implant's surface and surrounding tissues and the implants' survival rates and long-time stability must be considered [2]. In addition, surface features are considered critical factors in improving osseointegration [2]. The surface properties affect the permanence and the stability of the implant in the host bone. Therefore, introducing superficial modifications can improve early bone healing at the implant-bone interface, preventing implant failure. The implant osseointegration can be improved by changing surface roughness, usually through grinding, blasting, and acid etching [1]. These treatments influence cell behavior, modulating their attachment and adhesion, expression of angiogenic and osteogenic markers, and extracellular matrix (ECM) deposition [1, 2]. In addition, porosity is also an important factor in the success of the osseointegration process [3]. However, the conventional methods used to obtain a rough surface do not allow the fabrication of a structure with a completely controlled external shape design [1–3].

Additive manufacturing (AM) could be an alternative approach to overcome this limitation [4]. AM permits generating a physical model directly from computer-aided design (CAD) data or from data provided by computer-based medical imaging technologies in a layer-by-layer manner to obtain a customized implant [5,6]. Unlike traditional turning methods, 3D-printed surfaces can be made directly with a superficial roughness. Therefore, they do not always require post-processing subtractive or additive treatments to achieve a rough topography [7]. Moreover, this technique permits the production of surfaces with an open porous topography and an interconnected pattern. Another advantage of 3D-printed implants is the ability to produce personalized dental implants that perfectly fit the patient's anatomy because the project file can begin with the merging of the patient's cone-beam radiographs and digital impressions [7]. Among laser-based AM techniques, selective laser melting (SLM) can control each layer's porosity and pore interconnectivity, size, shape, and distribution, and thereby the 3D architecture of the implant [5,8–14].

Previous studies have shown that laser-based methods permit the production of dental implants that integrate well with the bone and soft tissue [8,15–18]. A prospective study by Mangano et al. showed an implant success rate of 97.8% after a one-year loading time [9]. Shibli et al. observed that direct laser-fabricated surfaces showed a higher bone-to-implant contact rate than machined surfaces after an eight-week healing period [12]. Mangano et al. found close contact with the human bone after an eight-week healing period [13]. A prospective three-year follow-up clinical study by Tunchel et al. evaluated the survival and success rates of 3D-printed and AM titanium dental implants, reporting a 94.5% survival rate and 94.3% implant-crown success rate [18].

Therefore, due to their high versatility, 3D printing technologies are applied in biomedical research for tissue and organ replacements and

drug delivery systems [7]. In addition, by monitoring several parameters in the implant design, 3D printing technology can control the macro-geometry to perfectly adapt the implant to the tissue defect and create customized implants with complex geometries that resemble endogenous tissues with analogous mechanical properties. An in vitro study has demonstrated that 3D-printed design and post-production treatments on titanium surfaces have a dynamic influence on dental pulp cell adhesion and osteogenic commitment [17]. Furthermore, histological studies have shown that 3D-printed implants are well integrated into bone with a high bone-to-implant contact [15,16].

Nevertheless, few studies have accounted for other aspects of the oral cavity beyond the osteogenic properties of a dental implant, and few have correlated the surface characteristics of 3D-printed dental implants with different cell responses [19]. Bioavailability and bioactivity are key aspects to consider. Therefore, human oral osteoblasts (hOBs), gingival fibroblasts (hGFs), mesenchymal stem cells (hAD-MSCs), and monocytes are the cells usually investigated to evaluate the biological properties of any tested surface [20]. The hOBs are relevant cells during implant rehabilitation due to their role in the anchorage of the dental implant. [21]. The hGFs act as a physical barrier to oral biofilm and protect the periodontium [22]. However, osseointegration needs to be supported by angiogenesis to have good dental implant stability [23]. One cell type involved in angiogenesis is hAD-MSCs, which show angiogenic properties and are involved in vessel development [24]. Nevertheless, a low risk of rejection after implant insertion should be considered, which is mediated by immune cells such as monocytes [25,26].

We have previously shown that different titanium surfaces produced by SLM and then subjected to organic acid etching (OAE) have a higher nano- and micro-roughness than SLM surfaces subjected to electrochemical polishing and traditional machined titanium [27,28]. These superficial features translated into a lower susceptibility of OAE-treated surfaces to colonization by pioneer bacteria. However, the biological response of host cells to these surfaces was not investigated [27,28]. Therefore, the first objective of this study was to characterize the surface topography of 3D-printed dental implants subjected to SLM and then to OAE at the micro- and macro-level using scanning electron microscopy (SEM). Its second objective was to investigate the SLM implants' osteogenic, angiogenic, and immunogenic properties. Therefore, it tested 3D-printed dental implants using the four cell types that usually play critical roles in the oral cavity: hOBs, hGFs, hAD-MSCs, and monocytes. The 3D-printed implants were compared to machined implants, which are traditionally used as controls in implant research.

## 2. Materials and methods

### 2.1. Study design

In this study, the test implant (TEST) was a laser-printed Ti64 Grade 23 dental implant (Andrew Medical srl, Carate Brianza, MB, Italy), and the control implant (CTRL) was a titanium dental implant with a machined surface (Fig. 1). First, the surface was characterized with a SEM microscope. Then, hOBs, hGFs, hAD-MSCs, and monocytes were cultured on half of the dental implant surface, placed into the well/plates, and then subjected to the following biological analyses:

- i Cell viability assessment with the 3-(4,5-dimethylthiazol-2-yl)–2,5-diphenyltetrazolium bromide (MTT) assay;
- ii Assessment of hOB and hGF adhesion and morphology using SEM and histological analyses;
- iii Assessment of adhesion-related marker gene expression in hAD-MSCs;
- iv Assessment of constitutive marker gene expression in hOBs and hGFs using real-time quantitative polymerase chain reactions (RT-qPCR);
- v Assessment of angiogenic and regenerative marker gene expression in hAD-MSCs;

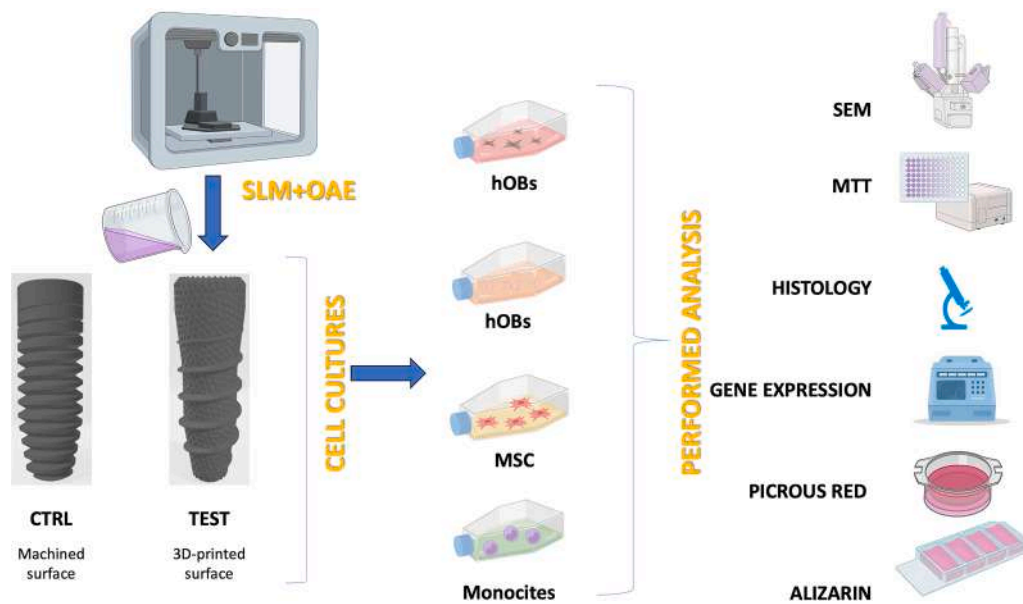


Fig. 1. Study design.

- vi Assessment of immune-related marker gene expression in monocytes;
- vii Assessment of mineralization by hOBs with alizarin red staining and spectrophotometric quantification;
- viii Assessment of collagen secretion by hGFs using picrosirius red staining and spectrophotometric analysis.

The laser-printed Ti64 Grade 23 dental implants were manufactured by the following procedure. The highest purity version of the Powder-Range Ti64 Grade 23 powder (6% titanium, 5% aluminum, vanadium; Ti-6Al-4 V; Carpenter Additive, Widnes, Cheshire, UK) was used with a RenAM 500Q printer (Renishaw, Wotton-under-Edge, Gloucestershire, UK). The PowderRange Ti64 Grade 23 powder is produced by plasma atomization, resulting in superior sphericity, low internal porosity, and low residual elements; the particle size is 10–20  $\mu\text{m}$ . Twenty porous titanium implants with a 4 mm diameter and 10 mm length were designed with an open cell form and interconnected pores using SolidWorks® 12.0 software (SolidWorks Corp., Waltham, MA, USA) and produced with a RenAM 500Q SLM printer equipped with four high power 500 W lasers that can access the entire powder bed surface simultaneously. Its compact galvanometer assembly was designed and additively manufactured in-house using aluminum due to its high thermal conductivity, including conformal cooling fluid channels, resulting in the excellent thermal stability of the optical system. The building parameters were a laser power of 200 W, a speed of 0.9 m/s, and a layer thickness of 15  $\mu\text{m}$ . Next, the laser-melted samples were vacuum heat-treated at 800 °C for 1 h. Then, the implants underwent post-processing OAE treatments. In order to remove the titanium spherical non-adherent particles from the surface, the samples underwent sonication for 5 min in deionized water at 25 °C, submerged in sodium hydroxide (20 g/L) and hydrogen peroxide (20 g/L) at 80 °C for 30 min, and then sonicated again for 5 min in deionized water. Then, the implants were OAE treatment in a 50% oxalic acid and 50% maleic acid mixture at 80 °C for 45 min to better clean the surface, followed by 5 min rinses with deionized water in a sonic bath, as previously reported [17] (Fig. 2).

## 2.2. SEM analysis

The dental implant surfaces were observed with SEM to characterize their surface. A Phenom ProX SEM (Phenom-World BV, Eindhoven, the Netherlands) was used with the element identification package (Phenom

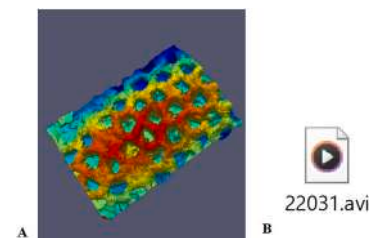


Fig. 2. A) Image of the 3D printed Ti6Al4V implant. B) The video opens with a SEM micrograph, taken from a stereo-pair, of a 3D-printed titanium implant (Supplementary video). The stereo-pair is then converted by dedicated software (Gallo et al., Pattern Recognition Letters 29, 673–687, 2008) into a 3D model suitable for interactive animation with standard computer graphics techniques. The dynamic depiction of the 3D model allows an immediate and more definite appreciation of the surface texture and of the depth of the cavities.

ProSuite Software; Phenom-World B.V.). Before observation, the samples were gold sputtered with a Desk Sputter Coater (Phenom-World B. V.). Images were captured using an accelerating voltage of 15 kV and a magnification of 300  $\times$ , 1000  $\times$ , or 1500  $\times$ .

## 2.3. Cell culture

The hOBs were extracted from bone fragments of patients treated at the Dental Clinic of the University Gabriele d'Annunzio Chieti-Pescara (Ethical Committee approval number: BONEISTO N. 22–10.07.2021) according to the protocol described by Pierfelice et al. [29]. The hGFs were obtained from the American Type Culture Collection (Manassas, VA, USA). Both cell lines were cultured on dental implant surfaces in Dulbecco's Modified Eagle low glucose medium (Corning, New York, NY, USA) supplemented with 10% fetal bovine serum (SIAL, Rome, Italy), 1% penicillin, and streptomycin (Corning) at 37 °C with 5% carbon dioxide ( $\text{CO}_2$ ). The hGFs and hOBs used were from the third and fifth passages.

The peripheral blood mononuclear cells (including monocytes) were isolated using the Ficoll–Paque gradient method. Briefly, fresh peripheral blood from patients was carefully poured into a tube at a 1:4 blood: Ficoll ratio, centrifuged at 591 g for 30 min at room temperature. The supernatant was discarded and the pellet containing the PBMCs was resuspended in 1 mL of PBS 1X for cell counting and viability tests. The

monocyte population was enriched by negative selection of unlabeled target cells using a human monocyte enrichment kit (EasySep, Stemcell Tech., France), according to the manufacturer's protocol. The cell cultures were maintained at 37 °C and 5% CO<sub>2</sub> and the medium was changed twice a week.

Human adipose hAD-MSCs (hAD-MSCs) were obtained from Lonza (Walkersville, MD, USA) and cultured in MSC Growth Medium (Bullet Kit, Lonza Inc.). Cell cultures were maintained at 37 °C with 5% CO<sub>2</sub>, and the medium was changed twice weekly.

#### 2.4. MTT assay

Cells were seeded onto the top of the dental implant surface at a density of  $5 \times 10^4$  cells/implant. The cells were incubated in direct contact with the implant for five days. Next, 0.5 mg/mL MTT solution (Sigma Aldrich, St. Louis, MO, USA) was added to each well, and the cells were incubated for 4 h at 37 °C with 5% CO<sub>2</sub>. Then, a solubilization solution was added to each well to dissolve the insoluble formazan. The spectrophotometrical absorbance was measured at 550 nm using a microplate reader (Synergy H1; Hybrid BioTek Instruments, Winooski, VT, USA). The MTT assessment involved five replicates and three independent analyses. The CTRL group comprised cells cultured on the machined surface.

#### 2.5. Cell attachment evaluation

The hOBs and hGFs were seeded onto the dental implant surface at a density of  $5 \times 10^4$  cells/implant and cultured for five days. Then, the cells were fixed with 2.5% glutaraldehyde (Thermo Fisher Scientific, Waltham, MA, USA) for 1 h and then dehydrated using increasing ethanol concentrations (Carlo Erba Reagents, Milano, Italy). The specimens were gold sputtered and observed using an SEM (XL20; Philips Inc., Eindhoven, The Netherlands) as previously described.

#### 2.6. Histological analysis

Cells were seeded onto the top of each dental implant at a density of  $5 \times 10^4$  cells/implant and cultured for five days. Next, each specimen was fixed with 10% buffered formalin (Sigma-Aldrich) and dehydrated using an increasing alcohol series (Carlo Erba Reagents). Then, they were embedded in a glycol methacrylate resin (Technovit 7200 VLC; Kulzer, Wehrheim, Germany) and polymerized. Finally, sections about 30 µm thick were stained with fuchsin and toluidine blue. The images were captured using an optical microscope (Leica, Wetzlar, Germany) at 200 × and 400 × magnification.

#### 2.7. Gene expression

RT-qPCR was used to evaluate the gene expression of osteocalcin (OCN), alkaline phosphatase (ALP), and bone morphogenetic protein 2 (BMP2) in hOBs and collagen 1 (COL1) and fibronectin 1 (FN1) in hGFs. Total RNA was isolated using the TriFast reagent (EuroClone, Pero, MI, Italy) and quantified using a Nanophotometer NP80 spectrophotometer (Implen NanoPhotometer, Westlake Village, CA, USA). Next, cDNA was synthesized using GoTaq® 2-Step RT-qPCR Kit (Promega, Madison, WI, USA). Then, SYBR Green (GoTaq® 2-Step RT-qPCR Kit; Promega) was used to perform RT-qPCR according to the manufacturer's instructions on a Quant Studio 7 Pro-Real-Time PCR System (Thermo Fisher Scientific). The results were normalized to β-actin (ACTB) for hOBs and glyceraldehyde-3-phosphate dehydrogenase (GAPDH) for hGFs using the 2<sup>-ΔCt</sup> method. The primer sequences are listed in Table 1.

Total RNA was isolated from hAD-MSCs and monocytes after 15 days of culturing on the TEST and CTRL implant surfaces using the total RNA Purification Plus kit (Norgen Biotek, Toronto, ON, Canada) to quantify gene expression. RNA quality and concentration were assessed with a NanoDrop™ ND-1000 spectrophotometer (Thermo Fisher Scientific).

**Table 1**

Primer sequences used in RT-qPCR.

Gene	Forward Primer (5'–3')	Reverse Primer (5'–3')
BMP2	GGAAGCAGCAACGCTAGAAG	GACTGCGGTCTCTAAAGGTC
OCN	TCAGCCAACCTCGTCACAGTC	GGCGTACCTGTATCAATGG
ALP	AATGAGTGAGTGACCATCCTGG	GCACCCAAGACCTGCTTTAT
COL1	AGTCAGAGTGAGGACAGTGAATTG	CACATCACACCAGGAAGTGC
FN1	GGAAAGTGCCCTATCTCTGATACC	AATGTTGGTGAATCGCAGGT
B-ACT	CCAGAGCGGTACAGGGATAG	GAGAAGATGACCCAGGACTCTC
GAPDH	ACGGGAAGCTTGTCAATCAAT	GGAGGGATCTCGATTCTT

For each sample, 500 ng of total RNA was reverse transcribed using an RT2 First Strand kit (Qiagen, Hilden, Germany) in a final reaction volume of 20 µL. Then, RT-qPCR was performed according to the user manual on a Human Wound Healing RT2 Profiler PCR Array (Qiagen) with a StepOnePlus™ Real-Time PCR System (Applied Biosystems, Foster City, CA, USA) using the RT2 SYBR Green ROX FAST Master Mix (Qiagen). The thermal cycling conditions were as follows: 95 °C for 10 min, followed by 40 cycles of 95 °C for 15 s, and 60 °C for 1 min. At the end of each run, a melting curve analysis was performed using the following program: 95 °C for 1 min, 65 °C for 2 min with the optics off, followed by increasing the temperature from 65 °C to 95 °C at 2 °C/min with the optics on. Each experiment was repeated three times, and each measure was repeated three times.

#### 2.8. Alizarin red staining and quantification of calcium deposits

The hOBs were seeded onto the implant surface at a density of  $5 \times 10^4$  cells/implant and cultured for 14 days at 37 °C with 5% CO<sub>2</sub>. Next, the specimens were fixed in 2.5% glutaraldehyde solution (Thermo Fisher Scientific) for 2 h. Then, alizarin red staining (ARS) solution (Sigma-Aldrich) was added and incubated for 1 h at room temperature before the excess dye was removed using deionized water. Then, images were captured using a camera. Next, 1 mL of 10% cetylpyridinium chloride (CPC; Sigma-Aldrich) was added to quantify calcium deposits through the chelation of calcium ions. After 1 h of incubation, the absorbance was measured at 540 nm using a microplate reader (Synergy H1 Hybrid; BioTek Instruments).

#### 2.9. Picrosirius red staining and spectrophotometric analysis

The hGFs were cultured on the top of each specimen at a density of  $5 \times 10^4$  cells/implant. Next, each sample was fixed in 2.5% glutaraldehyde (Thermo Fisher Scientific) for 2 h. Then, they were washed with phosphate-buffered saline and incubated in the staining solution (Sigma-Aldrich) at room temperature for 1 h. Next, the staining solution was removed, and the cells were washed three times with 0.1 N acetic acid (Carlo Erba Reagents). Then, the images were captured using a camera. For spectrophotometric analysis, picrosirius red was eluted in 0.1 N sodium hydroxide (Sigma-Aldrich) by adding 200 µL/well and incubating the plates on a rocking platform at room temperature for 1 h. Finally, the optical density at 540 nm was measured using a microplate reader (Synergy H1 Hybrid; BioTek Instruments).

#### 2.10. Statistical analysis

All experiments were performed in biological triplicates and repeated three times. The data are reported as means ± standard deviations (SDs). Statistical analyses were performed using GraphPad Prism 8 software (GraphPad Software, San Diego, CA, USA). Data were compared between groups using analysis of variance with Tukey's post hoc test. A *p*-value <0.05 was considered statistically significant.

### 3. Results

#### 3.1. Evaluation of dental implant surface topography

The observations at  $300\times$  showed a smooth surface in the CTRL group but a surface characterized by numerous pores in the TEST group. The pores were shown in detail at  $1000\times$  and  $1500\times$  magnification (Fig. 3).

#### 3.2. Proliferation of hGFs, hOBs, hAD-MSCs, and monocytes on dental implant surfaces

After culturing for five days, hOBs had proliferated significantly more on the TEST surface than on the CTRL surface ( $p < 0.0001$ ; Fig. 4A). The growth rate differed by  $+38.76\% \pm 8.14\%$ . In contrast, after five days of culturing, hGF proliferation was only slightly higher on the TEST surface than on the CTRL surface, and the difference was nonsignificant (Fig. 4B). However, hAD-MSC proliferation was significantly higher on the TEST surface than on the CTRL surface ( $p < 0.0001$ ; Fig. 4C), while monocyte proliferation was slightly lower on the TEST surface than on the CTRL surface (Fig. 4D).

#### 3.3. hOB and hGF attachment to the dental implant surface

The hOBs and hGFs showed excellent adhesion to the tested dental implants (Fig. 5-6). Specifically, hOBs and hGFs colonized the entire surface of the CTRL group, reaching the confluence of cells on the implants. In the TEST group, hOBs and hGFs grew particularly in the pores. At  $1000\times$  and  $1500\times$ , the cells were observed to interact through cellular extensions. Both cell types showed good morphology when adhered to the implant surface. Their shape appeared as a spindle, and they created a dense network. No dead hOBs were visible on the TEST surfaces, indicating their excellent cell viability (Fig. 5). The hGFs showed elongated and spindle shapes with cytoplasmic extensions and lamellipodia at  $1000\times$  and  $1500\times$  (Fig. 6).

#### 3.4. Histological analysis

The histological observations showed that hOBs adhered to the profile of the CTRL implant. While fewer hOBs were observed in the TEST group, they showed a typical hOB shape (Fig. 7). A similar situation was observed for hGFs. They colonized the profile of the machined surface (CTRL) and showed a typical morphology in the TEST group (Fig. 8).

#### 3.5. Gene expression

##### 3.5.1. Gene expression in hOBs and hGFs cultured on the dental implants

Figs. 9–10 show that the CTRL implants did not influence *OCN*, *ALP*, *BMP2*, *COL1*, and *FN1* expression. However, after five days of culturing, *OCN* expression in hOBs was significantly higher in the TEST group than in the CTRL group (Fig. 9A). Similarly, after 10 days of culturing, the increase in *OCN* expression was significantly greater in the TEST group than in the CTRL group ( $p < 0.0001$ ; Fig. 9A). *ALP* expression was also significantly higher in the TEST group than in the CTRL group ( $p < 0.0001$ ), increasing up to threefold after only 10 days of culturing ( $p < 0.0001$ ; Fig. 9B). *BMP2* expression increased significantly in a time-dependent manner after five days ( $p < 0.05$ ) and 10 days ( $p < 0.001$ ) of culturing (Fig. 9C). After five days, hGFs cultured on the CTRL and TEST surfaces showed similar *COL1* expression levels (Fig. 10A). However, *COL1* expression was significantly higher in the TEST group than in the CTRL group after 10 days of culturing ( $p < 0.001$ ; Fig. 10A). *FN1* expression increased significantly in a time-dependent manner after five and 10 days of culturing ( $p < 0.0001$ ; Fig. 10B).

##### 3.5.2. Gene expression of integrins in hAD-MSCs

The increased attachment of hAD-MSCs in the TEST group was also evaluated by quantifying the expression of genes encoding proteins related to cell attachment, such as integrins. The expression of collagen type 4 and 14 related to the early ECM secretion was several times higher in the TEST group than in the CTRL group ( $p < 0.0001$ ; Fig. 11).

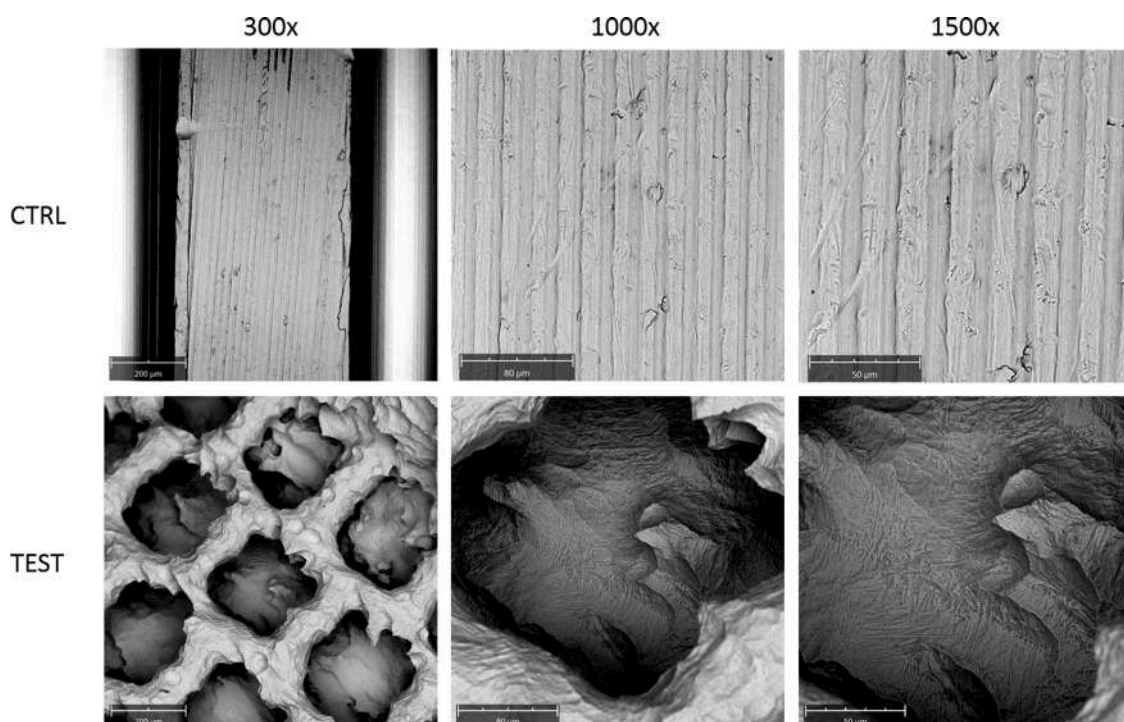


Fig. 3. Characterization of topography of dental implant surfaces at SEM. Magnification: 300, 1000 and 1500x.

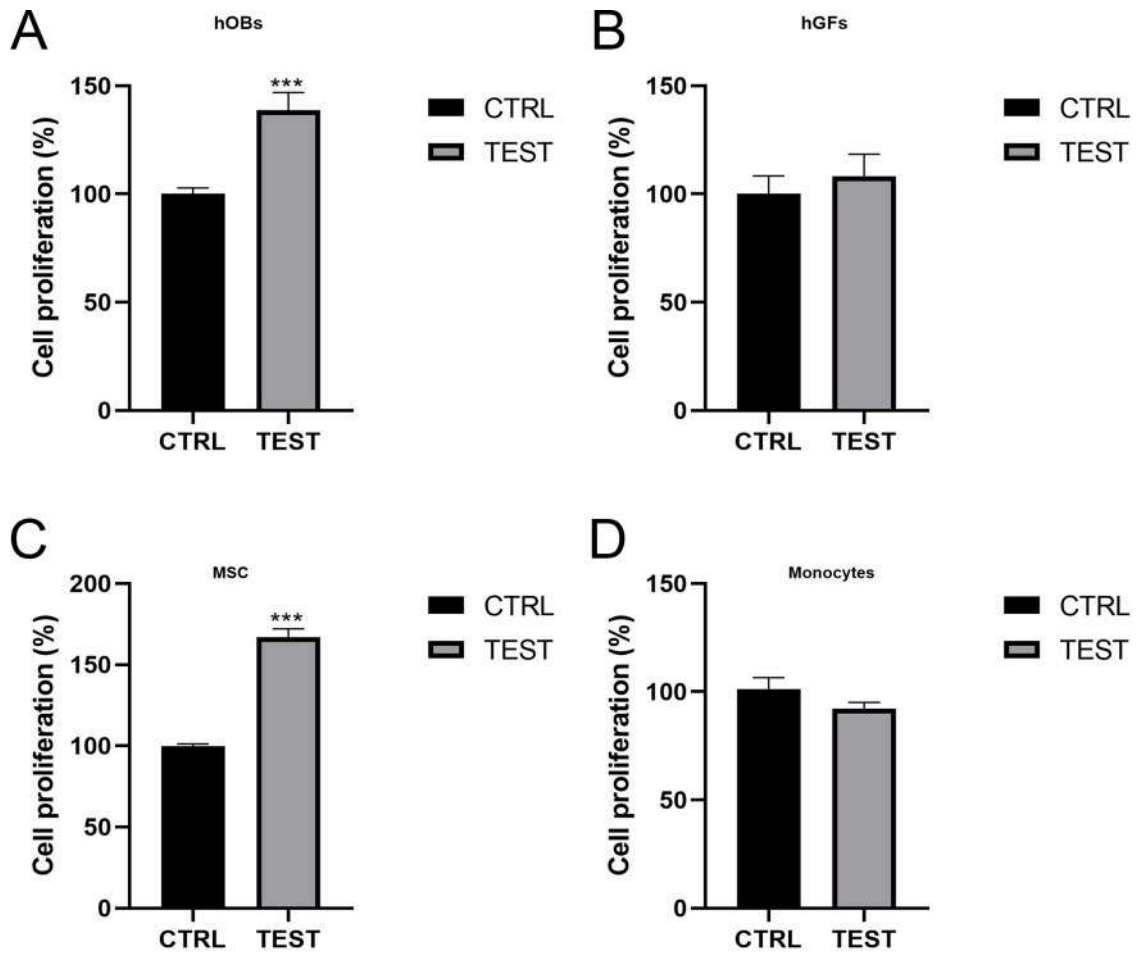


Fig. 4. Cell proliferation after 5 days of culture of hOBs (A), hGFs (B), MSC (C), monocytes (D) on the dental implant surfaces. (\*\*\*)  $p < 0.0001$  compared to CTRL).

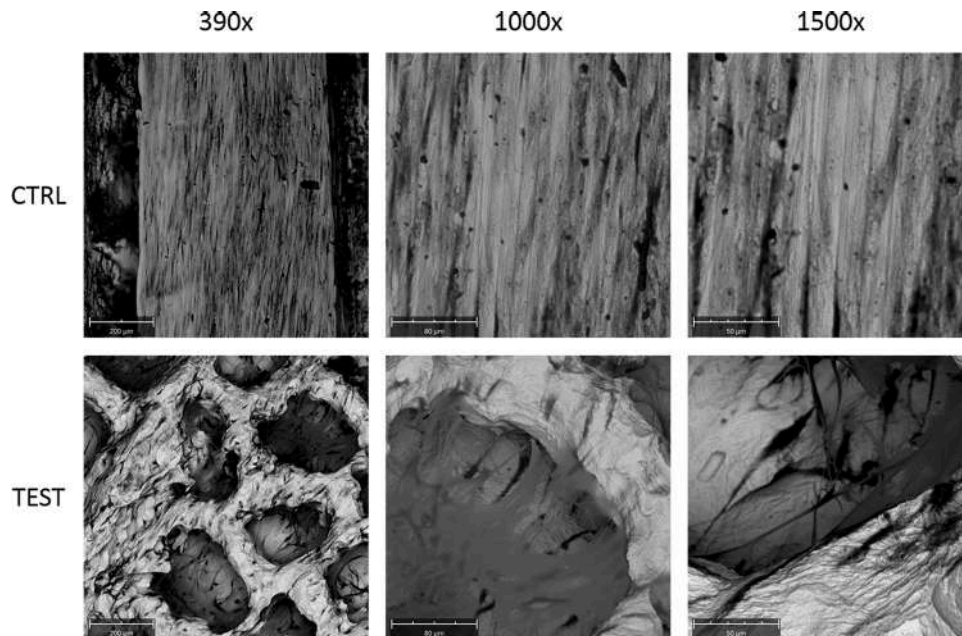


Fig. 5. SEM images of oral osteoblasts (hOBs) cultured on the tested dental implant surfaces at 5 days of culture. Magnification: 300, 1000 and 1500x.

### 3.5.3. Angiogenic potential

The angiogenic potential of the TEST group was evaluated based on gene expression in hAD-MSCs seeded onto the dental implant surfaces.

The gene expression of the principal angiogenesis-related markers, such as vascular endothelial growth factor A (*VEGFA*), platelet and endothelial cell adhesion molecule 1 (*PECAM1/CD31*), and von Willebrand

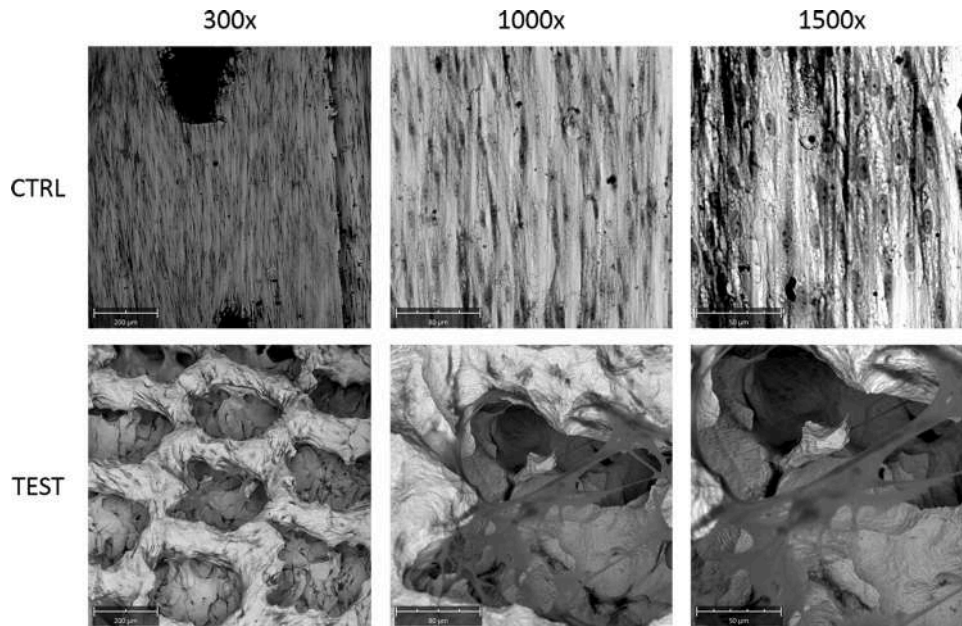


Fig. 6. SEM images of gingival fibroblasts (hGFs) cultured on the tested dental implant surfaces at 5 days of culture. Magnification: 300, 1000 and 1500x.

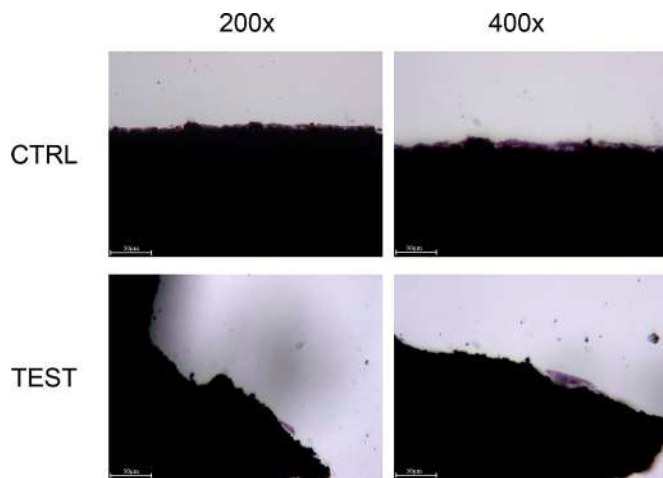


Fig. 7. hOBs morphology and adhesion evaluated by histological analysis at 5 days. Magnification: 200x, 400x.

factor (VWF), was evaluated after 15 days. *VEGFA* ( $p < 0.0001$ ), *VWF* ( $p < 0.0001$ ), and *CD31* ( $p < 0.01$ ) expression were significantly higher in the TEST group than in the CTRL group (Fig. 12).

### 3.5.4. Regenerative potential

The regenerative potential of the TEST group was evaluated based on gene expression in hAD-MSCs of all surface markers that indicate a state ready to be activated for tissue regeneration. The gene expression of these markers were several times higher in hAD-MSCs cultured on the TEST group than on the CTRL group (Fig. 13).

### 3.5.5. Immunomodulative potential

Monocytes cultured on TEST and CTRL dental implant surfaces could acquire an inflammatory (M1) or anti-inflammatory (M2) phenotype. The TEST dental implant surfaces directed monocytes more toward the M2 phenotype, mainly by increasing the expression of its related microRNAs (miRNAs; Fig. 14).

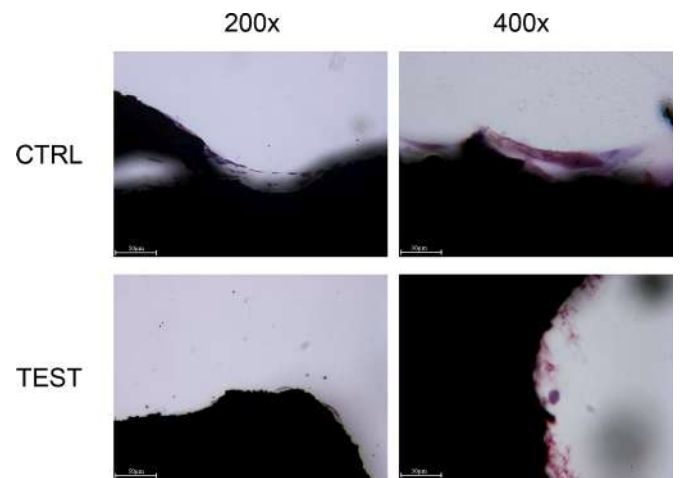


Fig. 8. hGFs adhesion and morphology evaluated by histological analysis at 5 days. Magnification: 200x, 400x.

### 3.6. Mineralization

The ARS images showed brighter red staining in the TEST group than in the CTRL group (Fig. 15A). The quantization with CPC confirmed the qualitative results. Therefore, significantly higher calcium deposition was observed in the TEST group than in the CTRL group ( $p < 0.0001$ ), differing by  $+42.75\% \pm 8.91\%$  (Fig. 15B).

### 3.7. Picrosirius red staining

The picrosirius red staining was visually similar in the CTRL and TEST groups (Fig. 16A). Nevertheless, the spectrophotometric analysis indicated slightly higher collagen production in the TEST group than in the CTRL group (Fig. 16B).

## 4. Discussion

This study compared the characteristics of a dental implant surface produced by combining 3D printing, SLM, and OAE post-processing with

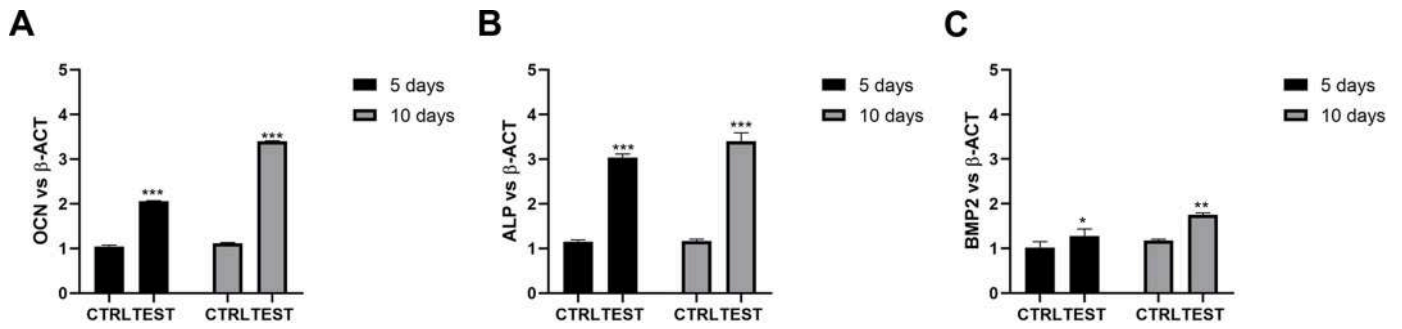


Fig. 9. Real-time PCR of osteoblasts seeded on dental implant surfaces for genes encoding (A) Osteocalcin (OCN), (B) Alkaline Phosphatase (ALP) and (C) Bone Morphogenetic Protein 2 (BMP2) at 5 and 10 days post seeding (\* $p < 0.05$ ; \*\* $p < 0.001$ ; \*\*\* $p < 0.0001$  compared to CTRL).

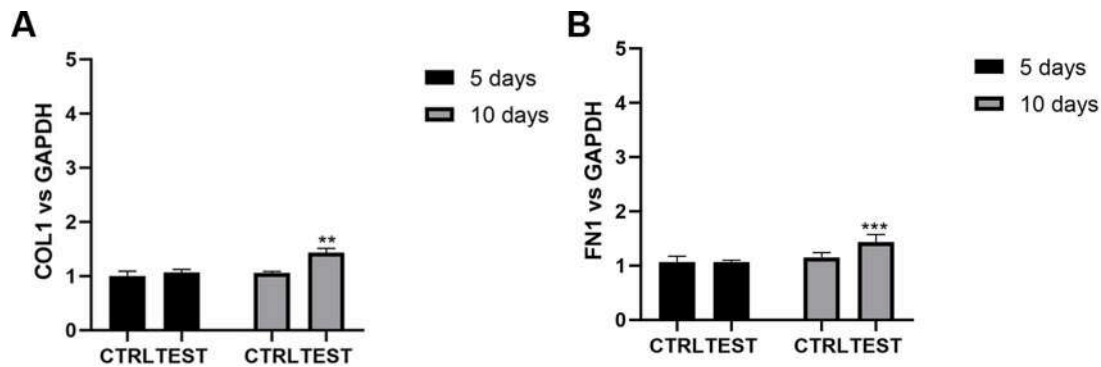


Fig. 10. Real-time PCR of gingival fibroblasts seeded on dental implant surfaces for genes encoding (A) Collagen 1 (COL1) and (B) Fibronectin 1 (FN1) at 5 and 10 days post seeding (\*\* $p < 0.001$ ; \*\*\* $p < 0.0001$  with respect to CTRL).

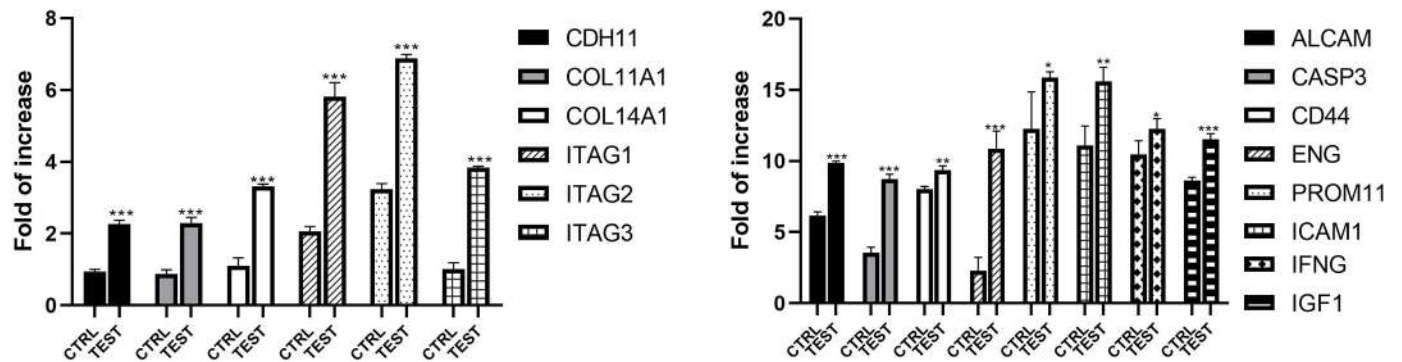


Fig. 11. Gene expression of extracellular matrix component related to the attachment onto the surfaces (\*\*\*)  $p < 0.0001$ .

Fig. 13. In gene expression of regenerative potential of MSC (\* $p < 0.05$ , \*\* $p < 0.001$ , \*\*\* $p < 0.0001$ ).

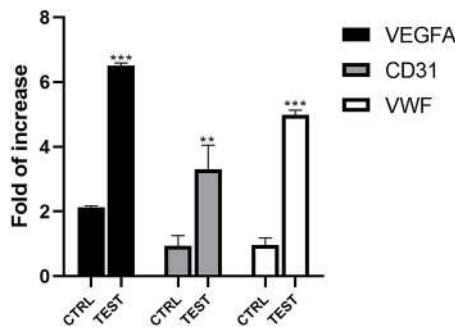


Fig. 12. In gene expression of angiogenic potential of MSC (\*\* $p < 0.001$ ; \*\*\* $p < 0.0001$ ).

those of a machined dental implant commonly used as the control in dental implant studies. SEM analysis showed that the tested implant had a higher surface roughness than the control surface, showing numerous peaks. A recent study reported that surface roughness is critical in promoting both osseointegration and the healing of tissues surrounding dental implants [30]. Histological studies demonstrated that roughened surfaces can favor faster bone healing than smooth surfaces [12,31]. Vaithilingam et al. demonstrated that specimens produced with SLM show a different surface roughness than those produced without SLM [32]. Because fibrin clot retention is crucial to the early stages of osseointegration, one study showed improved human blood fibrin clot extension on surfaces fabricated with SLM due to its higher micro-roughness [5].

In our study, besides roughness, SEM images showed that the tested implant had a highly porous structure with an open cell form due to the interconnected pores obtained by combining 3D CAD data with SLM.

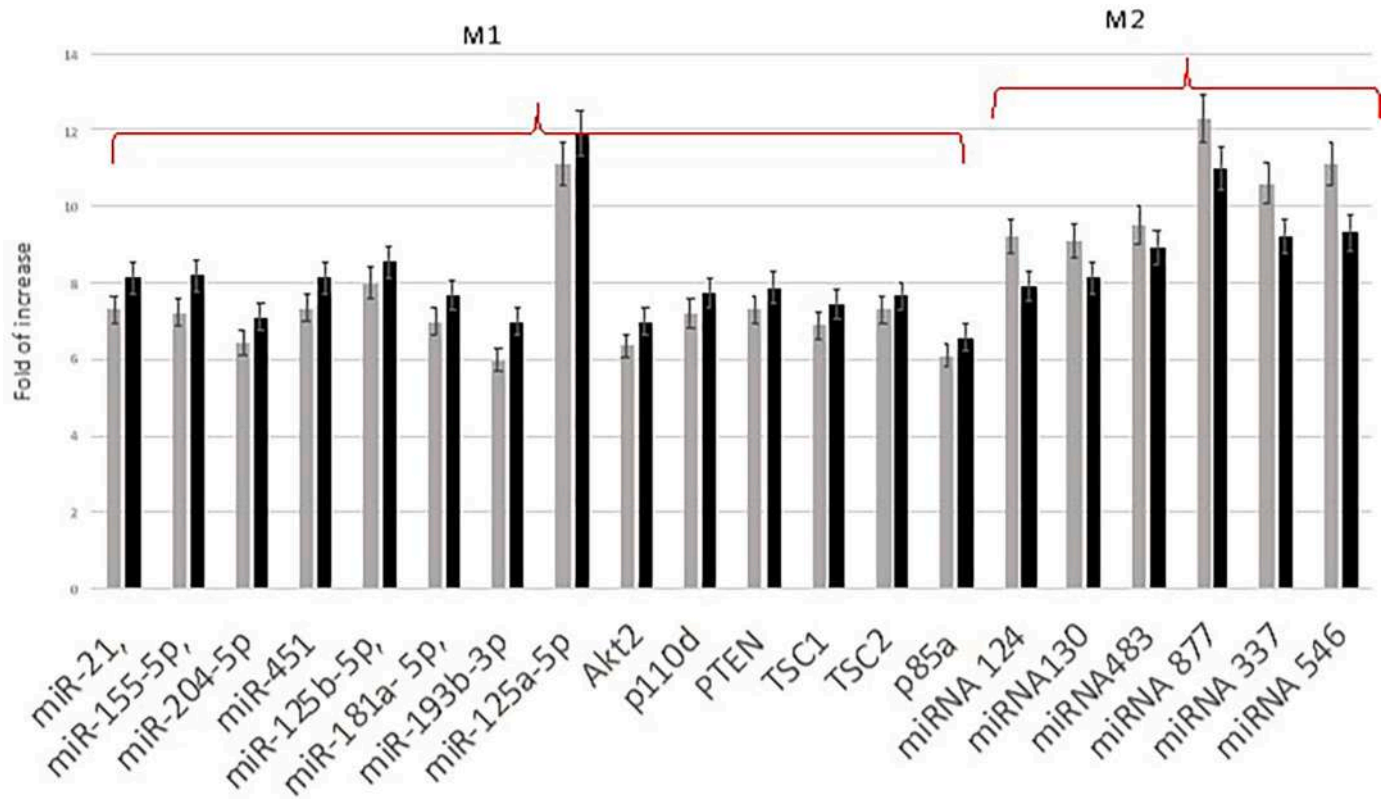


Fig. 14. In gene expression of immunomodulative potential of MSC: black columns are related to machined surfaces (CTRL) and gray related to TEST. As reported miRNA related to M1 inflammatory phenotype are down regulated into test culture compared to the same cultures onto machined one. By contrast into the tested surface, miRNA expression related to M2 macrophages phenotype are up regulated.

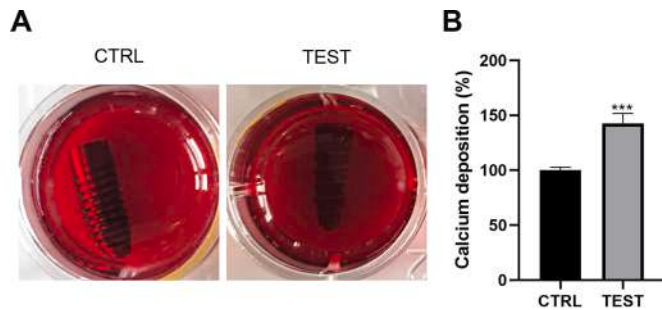


Fig. 15. Mineralization of hOBs at 14 days of culture on the dental implants. (A) Qualitative evaluation by Alizarin red staining, (B) Quantitative evaluation by CPC. (\*\*\*)  $p < 0.0001$ .

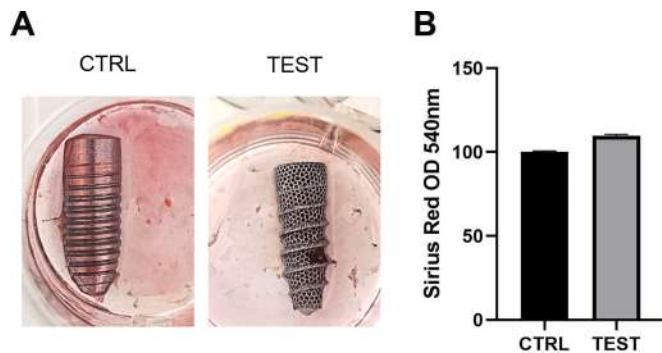


Fig. 16. In vitro Picosirius red staining was used to evaluate the production of collagen at 5 days of culture in hGFs.

Another study exploring the mechanical properties of different porous implant surfaces showed that a 3D-printed Ti-6Al-4 V porous implant had an elastic modulus closer to the human bone than conventional porous implants [11]. Other studies have reported that 3D-printed porous interconnectivity improves implant osseointegration by promoting bone ingrowth [33]. A three-year multicenter study by Tunchel et al. successfully rehabilitated single-tooth gaps in both jaws using 3D-printed titanium dental implants [18].

After characterizing the surface properties, we cultured hOBs, hGFs, hAD-MSCs, and monocytes on nonporous machined and porous roughened 3D-printed implants and examined their morphology, vitality, proliferation, and behavior. The hOBs and hGFs isolated from oral tissues were chosen due to their fundamental role in the two main tissues in the oral cavity: hard and connective, respectively. The hOB response to a dental implant generally implies an initial cell attachment and spreading phase, followed by the proliferation and differentiation phase with consequent ECM deposition and bone matrix mineralization [34]. Therefore, the cell-implant interaction is the critical step affecting the second phase, meaning that a stable cell attachment is fundamental for further proliferation and bone formation. Consequently, hOB adhesion and morphology were first investigated through histological and SEM analyses. After five days of cell culturing on the implants, histological and SEM images showed appreciable differences in hOB adherence between the porous 3D-printed test implant and the nonporous machined control implant, which also spread into the pores. The porous 3D-printed implant is accurately designed to mimic the porous structure of bone tissue. SEM images showed numerous hOBs had infiltrated and adhered within the huge pores of the 3D-printed test implant. These results were consistent with the cell viability data that showed significantly higher hOB proliferation on the 3D-printed test implant than on the machined control implant after five days of culturing, which can be attributed to its higher roughness surface and pores.

Each phase of the hOBs response to implants involved expressing and regulating distinct genes. BMP2 acts as an inducer of bone formation by exerting its stimulatory effect on hOB differentiation [35]. In our study, *BMP2* expression was time-dependent and significantly higher in those seeded on the porous 3D-printed test implant. *BMP2* expression has been associated with those of the bone cell differentiation marker genes *ALP*, *OCN*, and osteopontin (*OPN*) [36]. *ALP* represents a marker of hOB proliferation and differentiation, with its expression increasing from the early to late hOB maturation stages [37]. In our study, *ALP* expression was higher in hOBs cultured on the 3D-printed test implant than on the machined control implant, with the greatest difference after 10 days. During bone matrix mineralization, *ALP* expression generally correlates with *OCN* expression [37]. Indeed, *ALP* and *OCN* were overexpressed at both time points, with the highest level after 10 days, indicating that peak *ALP* and *OCN* expression marked the maturation of the bone matrix, and the formation of calcium nodules observed and quantified after 14 days indicated bone matrix mineralization. Altogether, the hOB-related results suggested that a porous and rougher surface was superior to a smooth surface in supporting hOB-triggered hard tissue integration by favoring cell attachment, proliferation, and expression of critical genes involved in bone formation and remodeling. These results are consistent with a previous study showing the biocompatibility and osteoconductive features of a 3D-printed porous implant in the presence of dental pulp mesenchymal cells [17]. Another recent study demonstrated the excellent mechanical properties of porous dental implants fabricated with magnesium alloy using SLM. This study also demonstrated the stimulatory effect of the porous implant on hOB proliferation [38].

Besides hOBs, dental implants usually interact with several other cell types, including hGFs. Numerous in vitro studies have demonstrated the osteogenic properties of SLM titanium implants. However, few studies have explored their interaction with soft tissue [17,38,39]. Since hGFs are the main cells involved in wound healing around the neck of the implant, we investigated hGFs cultured on the surface of the porous 3D-printed test implant. The macro and micro characteristics of the 3D-printed test implant seemed to favor hGF attachment and spread compared to the machined control implant. The cell viability assay showed a greater proliferation effect with the 3D-printed porous test implant than with the nonporous machined control implant. However, the difference was nonsignificant, indicating only good biocompatibility.

Our results also demonstrated that porous implants could significantly promote the expression of the main hGF genes, including *COL1* and *FN1*, after 10 days of culturing. Since hGFs secrete ECM components, mainly collagen, we investigated collagen production through picrosirius staining. Altogether, our data and images suggested that the micro and macro characteristics of the 3D-printed implant with a rough and porous surface provided a more favorable environment for hGF adhesion and secretion of ECM proteins than the nonporous machined control implant. An in vitro study on a superhydrophilic 3D-printed titanium implant reported similar results, showing that it significantly promoted the early adhesion and proliferation of HGFs [40].

The osseointegration process can not occur properly in vivo without three preceding events: vascularization, cell tissue regeneration, and inflammation cessation [41]. Vasculogenesis was activated by the 3D-printed surface, reflected by the increased expression of genes related to endothelial physiology, including *VEGFA*, *CD31*, and *VWF* [42]. Tissue regeneration involves new ECM synthesis and increases in markers related to cell interactions with collagen type I and hyaluronic acid. hAD-MSCs cultured on the 3D-printed test implant surface showed increased expression of receptors related to the interaction with hyaluronic acid: *CD44*, activated leukocyte cell adhesion molecule (*ALCAM*), endoglin (*ENG*), and intercellular adhesion molecule 1 (*ICAM*), which increase vascular derived cell adhesion, and insulin-like growth factor 1 (IGF1), mainly increases hOB proliferation and activation [43,44]. The inflammatory process is preparatory to preparing a clean tissue, prime of

necrotic debris to enhance the synthesis of a new ECM. The main actors in this process are neutrophils and macrophages that must switch from an initial inflammatory (M1) to an anti-inflammatory (M2) phenotype that initiates subsequent angiogenic processes [45,46]. Our results demonstrated that the 3D-printed test implant facilitated this change by the increased gene expression of all markers related to acquiring the M2 phenotype in monocytes cultured on its surface, especially the miRNAs 124, 130, 483, 877, 337, and 546 [47].

Altogether, our results suggest that SLM, an AM technology applied to 3D printing, is a promising method for producing dental implants from titanium alloys with structural characteristics close to bone structure. The main advantage of SLM is the ability to fabricate dental implants with anatomical requirements, such as a microarchitecture with high porosity and interconnectivity [7,11]. The highly interconnected porous architecture of the 3D-printed test implant seems to represent a 3D system with osteogenic, angiogenic, and immunogenic properties. The additional acid surface treatments to remove weakly adherent metal particles make the surface more suitable for cell attachment and proliferation [48,49]. This type of post-processing method, such as OAE or electrochemical polishing, could represent a limitation of 3D-printed implants due to different bacterial contamination, as we have previously shown [27,28]. However, D'Ercole et al. showed that a highly porous titanium surface produced by selective laser sintering and treated by OAE showed high anti-adhesive and anti-bacterial properties [27].

Within the limits of our study, the 3D-printed titanium dental implants might be a successful clinical option for rehabilitating single-tooth gaps. However, their corrosion resistance under various pH and physiological conditions remained to be assessed. In addition, their mechanical resistance and stability must be examined over an extended period to ensure clinical translation. Nevertheless, while machining, blasting, grinding, and polishing techniques have been used to obtain controlled micro-scale surface topographies on dental implants, attrition can be used to produce nano-scale layers to improve mechanical characteristics, such as hardness and wettability.

## Conclusions

In conclusion, SLM-fabricated 3D implants with OAE surfaces showed improved cellular interaction and functions compared to machined controls. The rougher surface obtained with OAE seemed to support higher cellular adhesion and proliferation than the machined control treatment. *OCN*, *ALP*, and *BMP2* expression were significantly higher in cells cultured on the 3D-printed test implant surface than those cultured on the machined control surface. Picrosirius red staining showed that the 3D-printed test implants induced higher collagen production than the machined test implants. In addition, hAD-MSCs showed increased expression of endothelial and osteogenic commitment-related markers, such as *VEGFA* and *COL1*. Moreover, monocytes showed increased expression of miRNAs related to the M2 macrophage phenotype. Based on these results, SLM-fabricated 3D implants with OAE surfaces show improved biological properties than traditional machined implants.

## Ethics approval

The study was conducted in accordance with the Declaration of Helsinki and approved by the Institutional Review Board (or Ethics Committee) of Ethical Committee of University G. d'Annunzio Chieti–Pescara protocol BONEISTO N. 22-10.07.2021.

## Disclosure instructions

Authors must disclose the use of generative AI and AI-assisted technologies in the writing process.

## Funding

This work was supported by G.I. FAR GRANT University of Chieti–Pescara Fund.

## CRediT authorship contribution statement

**Giovanna Iezzi:** Conceptualization, Methodology, Software, Supervision. **Barbara Zavan:** Conceptualization, Methodology, Software, Supervision. **Morena Petrini:** Data curation, Writing – original draft, Visualization, Investigation, Writing – review & editing. **Letizia Ferroni:** Data curation, Writing – original draft, Visualization, Investigation, Writing – review & editing. **Tania Vanessa Pierfelice:** Data curation, Writing – original draft. **Ugo D’Amora:** Software, Validation, Writing – review & editing. **Alfredo Ronca:** Visualization, Investigation, Writing – review & editing. **Emira D’Amico:** Data curation, Writing – original draft, Visualization, Investigation, Software, Validation, Writing – review & editing. **Carlo Mangano:** Conceptualization, Methodology, Software, Supervision.

## Declaration of Competing Interest

No conflict of interest is reported. No financial support was obtained for conducting the present investigation.

## Acknowledgment

Tania Vanessa Pierfelice has a Ph.D. program fellowship (code n. DOT1353500) in the framework of PON RI 201/2020, Action I.1-“Innovative PhDs with industrial characterization”, funded by the Ministry of University and Research (MUR), Italy, FSE-FESR. Graphical abstract was created with BioRender.com.

## Supplementary materials

Supplementary material associated with this article can be found, in the online version, at [doi:10.1016/j.jdent.2023.104778](https://doi.org/10.1016/j.jdent.2023.104778).

## References

- [1] C. Nelson, Factors affecting the success of dental implants. *Implant Dentistry - A Rapidly Evolving Practice*, 2011, <https://doi.org/10.5772/18746>.
- [2] R. Smeets, B. Stadlinger, F. Schwarz, B. Beck-Broichsitter, O. Jung, C. Precht, F. Kloss, A. Gröbe, M. Heiland, T. Ebker, Impact of dental implant surface modifications on osseointegration, *Biomed. Res. Int.* 2016 (2016), <https://doi.org/10.1155/2016/6285620>.
- [3] G. Ryan, A. Pandit, D.P. Apatsidis, Fabrication methods of porous metals for use in orthopaedic applications, *Biomaterials* 27 (2006) 2651–2670, <https://doi.org/10.1016/j.biomaterials.2005.12.002>.
- [4] C. Mangano, F. Mangano, J.A. Shibli, G. Luongo, M. De Franco, F. Briguglio, M. Figliuzzi, T. Eccellente, C. Rapani, M. Piombino, A. MacChi, Prospective clinical evaluation of 201 direct laser metal forming implants: results from a 1-year multicenter study, *Lasers Med. Sci.* 27 (2012) 181–189, <https://doi.org/10.1007/S10103-011-0904-3>.
- [5] C. Mangano, M. Raspanti, T. Traini, A. Piattelli, R. Sammons, Stereo imaging and cytocompatibility of a model dental implant surface formed by direct laser fabrication, *J. Biomed. Mater. Res. A* 88 (2009) 823–831, <https://doi.org/10.1002/JBM.A.32033>.
- [6] F. Mangano, L. Chambrone, R. Van Noort, C. Miller, P. Hatton, C. Mangano, Direct metal laser sintering titanium dental implants: a review of the current literature, *Int. J. Biomater.* 2014 (2014), <https://doi.org/10.1155/2014/461534>.
- [7] A. Louvrier, P. Marty, A. Barrabé, E. Euvrard, B. Chatelain, E. Weber, C. Meyer, How useful is 3D printing in maxillofacial surgery? *J. Stomatol. Oral Maxillofac. Surg.* 118 (2017) 206–212, <https://doi.org/10.1016/J.JORMAS.2017.07.002>.
- [8] C. Mangano, A. Piattelli, A. Scarano, M. Raspanti, J. Shibli, F. Mangano, V. Perrotti, G. Iezzi, A light and scanning electron microscopy study of human direct laser metal forming dental implants, *Int. J. Periodont. Restorative Dent.* 34 (2014) e9–e17, <https://doi.org/10.11607/PRD.1213>.
- [9] C. Mangano, F.G. Mangano, J.A. Shibli, M. Ricci, V. Perrotti, S. d’Avila, A. Piattelli, Immediate loading of mandibular overdentures supported by unsplinted direct laser metal-forming implants: results from a 1-year prospective study, *J. Periodontol.* 83 (2012) 70–78, <https://doi.org/10.1902/JOP.2011.110079>.
- [10] F. Mangano, S. Pozzi-Taubert, P.A. Zecca, G. Luongo, R.L. Sammons, C. Mangano, Immediate restoration of fixed partial prostheses supported by one-piece narrow-diameter selective laser sintering implants: a 2-year prospective study in the posterior jaws of 16 patients, *Implant Dent.* 22 (2013) 388–393, <https://doi.org/10.1097/ID.0B013E31829AFA9D>.
- [11] T. Traini, C. Mangano, R.L. Sammons, F. Mangano, A. Macchi, A. Piattelli, Direct laser metal sintering as a new approach to fabrication of an isoelastic functionally graded material for manufacture of porous titanium dental implants, *Dent. Mater.* 24 (2008) 1525–1533, <https://doi.org/10.1016/J.DENTAL.2008.03.029>.
- [12] J.A. Shibli, C. Mangano, S. D’Avila, A. Piattelli, G.E. Pecora, F. Mangano, T. Onuma, L.A. Cardoso, D.S. Ferrari, K.C. Aguiar, G. Iezzi, Influence of direct laser fabrication implant topography on type IV bone: a histomorphometric study in humans, *J. Biomed. Mater. Res. A* 93 (2010) 607–614, <https://doi.org/10.1002/JBM.A.32566>.
- [13] C. Mangano, A. Piattelli, M. Raspanti, F. Mangano, A. Cassoni, G. Iezzi, J.A. Shibli, Scanning electron microscopy (SEM) and X-ray dispersive spectrometry evaluation of direct laser metal sintering surface and human bone interface: a case series, *Lasers Med. Sci.* 26 (2011) 133–138, <https://doi.org/10.1007/S10103-010-0831-8>.
- [14] F. Mangano, C. Mangano, Laser sintering in dentistry. *Handbook of Surgical Planning and 3D Printing: Applications, Integration, and New Directions*, 2023, pp. 203–227, <https://doi.org/10.1016/B978-0-323-90850-4.00005-3>.
- [15] J.A. Shibli, C. Mangano, F. Mangano, J.A. Rodrigues, A. Cassoni, K. Bechara, J.D. B. Ferreira, A.M. Dottore, G. Iezzi, A. Piattelli, Bone-to-implant contact around immediately loaded direct laser metal-forming transitional implants in human posterior maxilla, *J. Periodontol.* 84 (2013) 732–737, <https://doi.org/10.1902/JOP.2012.120126>.
- [16] F. Mangano, C. Mangano, A. Piattelli, G. Iezzi, Histological evidence of the osseointegration of fractured direct metal laser sintering implants retrieved after 5 years of function, *Biomed. Res. Int.* 2017 (2017), <https://doi.org/10.1155/2017/9732136>.
- [17] M. Gallorini, S. Zara, A. Ricci, F.G. Mangano, A. Cataldi, C. Mangano, The open cell form of 3D-printed titanium improves osteoconductive properties and adhesion behavior of dental pulp stem cells, *Materials (Basel)* 14 (2021), <https://doi.org/10.3390/MA14185308>.
- [18] S. Tunchel, A. Blay, R. Kolerman, E. Mijiritsky, J.A. Shibli, 3D printing/additive manufacturing single titanium dental implants: a prospective multicenter study with 3 years of follow-up, *Int J Dent* 2016 (2016), <https://doi.org/10.1155/2016/8590971>.
- [19] U.L. Lee, S. Yun, H. Lee, H.L. Cao, S.H. Woo, Y.H. Jeong, T.G. Jung, C.M. Kim, P. H. Choung, Osseointegration of 3D-printed titanium implants with surface and structure modifications, *Dent. Mater.* 38 (2022) 1648–1660, <https://doi.org/10.1016/J.DENTAL.2022.08.003>.
- [20] Nagy Abdulsamee, Biocompatibility of dental implant: revised, (2021). [https://www.academia.edu/76381610/Biocompatibility\\_of\\_Dental\\_Implant\\_Revision](https://www.academia.edu/76381610/Biocompatibility_of_Dental_Implant_Revision) (accessed September 5, 2023).
- [21] X. Gao, M. Fraulob, G. Häät, Biomechanical behaviours of the bone-implant interface: a review, *J. R. Soc. Interface* 16 (2019), <https://doi.org/10.1098/RSIF.2019.0259>.
- [22] V. Pivodovaa, J. Frankovaa, J. Ulrichovaa, Osteoblast and gingival fibroblast markers in dental implant studies, *Biomed. Pap. Med. Fac. Univ. Palacky Olomouc Czech Repub.* 155 (2011) 109–116, <https://doi.org/10.5507/BP.2011.021>.
- [23] A.L. Raines, R. Olivares-Navarrete, M. Wieland, D.L. Cochran, Z. Schwartz, B. D. Boyan, Regulation of angiogenesis during osseointegration by titanium surface microstructure and energy, *Biomaterials* 31 (2010) 4909–4917, <https://doi.org/10.1016/J.BIOMATERIALS.2010.02.071>.
- [24] S.M. Watt, F. Gullo, M. Van Der Garde, D. Markeson, R. Camicia, C.P. Khoo, J. J. Zwaginga, The angiogenic properties of mesenchymal stem/stromal cells and their therapeutic potential, *Br. Med. Bull.* 108 (2013) 25–53, <https://doi.org/10.1093/BMB/LDT031>.
- [25] M. Baseri, F. Radmand, R. Hamed, M. Yousefi, H.S. Kafil, Immunological aspects of dental implant rejection, *Biomed. Res. Int.* 2020 (2020), <https://doi.org/10.1155/2020/7279509>.
- [26] V. Bordonio, G. Reina, M. Orecchioni, G. Furesi, S. Thiele, C. Gardin, B. Zavan, G. Cuniberti, A. Bianco, M. Rauner, L.G. Delogu, Stimulation of bone formation by monocyte-activator functionalized graphene oxide in vivo, *Nanoscale* 11 (2019) 19408–19421, <https://doi.org/10.1039/C9NR03975A>.
- [27] S. D’ercole, C. Mangano, L. Cellini, S. Di Lodovico, C.A. Ozkaya, G. Iezzi, A. Piattelli, M. Petrini, A novel 3D titanium surface produced by selective laser sintering to counteract streptococcus oralis biofilm formation, *Appl. Sci.* 2021 11 (2021) 11915, <https://doi.org/10.3390/AP112411915>. Page111915.
- [28] M. Petrini, C. Mangano, L. Cellini, M. Di Giulio, G. Iezzi, A. Piattelli, S. D’Ercole, Material characterization and bacterial interaction of titanium discs produced by selective laser melting, *Mater. Charact.* 189 (2022), 111989, <https://doi.org/10.1016/J.MATCHAR.2022.111989>.
- [29] T.V. Pierfelice, E. D’amico, G. Iezzi, A. Piattelli, N. Di Pietro, C. D’arcangelo, L. Comuzzi, M. Petrini, Nanoporous titanium enriched with calcium and phosphorus promotes human oral osteoblast bioactivity, *Int. J. Environ. Res. Public Health* 2022 19 (2022) 6212, <https://doi.org/10.3390/IJERPH19106212>. Page196212.
- [30] G.R.M. Matos, Surface roughness of dental implant and osseointegration, *J. Maxillofac. Oral Surg.* 20 (2021), <https://doi.org/10.1007/S12663-020-01437-5>.
- [31] J.A. Shibli, S. Grassi, A. Piattelli, G.E. Pecora, D.S. Ferrari, T. Onuma, S. D’Avila, P. G. Coelho, R. Barros, G. Iezzi, Histomorphometric evaluation of bioceramic molecular impregnated and dual acid-etched implant surfaces in the human posterior maxilla, *Clin. Implant Dent. Relat. Res.* 12 (2010) 281–288, <https://doi.org/10.1111/J.1708-8208.2009.00174.X>.

- [32] J. Vaithilingam, E. Prina, R.D. Goodridge, R.J.M. Hague, S. Edmondson, F.R.A. J. Rose, S.D.R. Christie, Surface chemistry of Ti6Al4V components fabricated using selective laser melting for biomedical applications, *Mater. Sci. Eng. C Mater. Biol. Appl.* 67 (2016) 294–303, <https://doi.org/10.1016/J.MSEC.2016.05.054>.
- [33] A. Jíra, M. Šejnoha, T. Krejčí, J. Vorel, L. Řehounek, G. Marseglia, Mechanical properties of porous structures for dental implants: experimental study and computational homogenization, *Materials (Basel)* 14 (2021), <https://doi.org/10.3390/MA14164592>.
- [34] K. Rabel, R.J. Kohal, T. Steinberg, P. Tomakidi, B. Rolauuffs, E. Adolfsson, P. Palmero, T. Fürderer, B. Altmann, Controlling osteoblast morphology and proliferation via surface micro-topographies of implant biomaterials, *Sci. Rep.* 10 (2020), <https://doi.org/10.1038/S41598-020-69685-6>.
- [35] V.S. Salazar, L.W. Gamer, V. Rosen, BMP signalling in skeletal development, disease and repair, *Nat. Rev. Endocrinol.* 12 (2016) 203–221, <https://doi.org/10.1038/NREND0.2016.12>.
- [36] J. Sun, J. Li, C. Li, Y. Yu, Role of bone morphogenetic protein-2 in osteogenic differentiation of mesenchymal stem cells, *Mol Med Rep* 12 (2015) 4230–4237, <https://doi.org/10.3892/MMR.2015.3954>.
- [37] J.F.L. Chau, W.F. Leong, B. Li, Signaling pathways governing osteoblast proliferation, differentiation and function, *Histol. Histopathol.* 24 (2009) 1593–1606, <https://doi.org/10.14670/HH-24.1593>.
- [38] X. Zhang, J. Mao, Y. Zhou, F. Ji, X. Chen, Mechanical properties and osteoblast proliferation of complex porous dental implants filled with magnesium alloy based on 3D printing, *J. Biomater. Appl.* 35 (2021) 1275–1283, <https://doi.org/10.1177/0885328220957902>.
- [39] K. Gulati, M. Prideaux, M. Kogawa, L. Lima-Marques, G.J. Atkins, D.M. Findlay, D. Losic, Anodized 3D-printed titanium implants with dual micro- and nano-scale topography promote interaction with human osteoblasts and osteocyte-like cells, *J. Tissue Eng. Regen. Med.* 11 (2017) 3313–3325, <https://doi.org/10.1002/TERM.2239>.
- [40] Y. Guo, X. Wang, C. Wang, S. Chen, In vitro behaviour of human gingival fibroblasts cultured on 3D-printed titanium alloy with hydrogenated TiO<sub>2</sub> nanotubes, *J. Mater. Sci. Mater. Med.* 33 (2022), <https://doi.org/10.1007/S10856-022-06649-4>.
- [41] M. Tatullo, A. Piattelli, B. Zavan, Regenerative Medicine, Role of stem cells and innovative biomaterials 2.0, *Int. J. Mol. Sci.* 23 (2022), <https://doi.org/10.3390/IJMS23084199>.
- [42] C. Gardin, L. Ferroni, Y.K. Erdoğan, F. Zanotti, F. De Francesco, M. Trentini, G. Brunello, B. Ercan, B. Zavan, Nanostructured modifications of titanium surfaces improve vascular regenerative properties of exosomes derived from mesenchymal stem cells: preliminary in vitro results, *Nanomaterials (Basel)* 11 (2021), <https://doi.org/10.3390/NANO11123452>.
- [43] E. Mijiritsky, C. Gardin, L. Ferroni, Z. Lacza, B. Zavan, Albumin-impregnated bone granules modulate the interactions between mesenchymal stem cells and monocytes under in vitro inflammatory conditions, *Mater. Sci. Eng. C Mater. Biol. Appl.* 110 (2020), <https://doi.org/10.1016/J.MSEC.2020.110678>.
- [44] F. Zanotti, I. Zanolta, M. Trentini, E. Tiengo, T. Pusceddu, D. Licastro, M. Degasperis, S. Leo, E. Tremoli, L. Ferroni, B. Zavan, Mitochondrial metabolism and EV cargo of endothelial cells is affected in presence of EVs derived from hAD-MSCs on which HIF is activated, *Int. J. Mol. Sci.* 2023 24 (2023) 6002, <https://doi.org/10.3390/IJMS24066002>. Page246002.
- [45] A. Ariano, F. Posa, G. Storlino, G. Mori, Molecules inducing dental stem cells differentiation and bone regeneration: state of the art, *Int. J. Mol. Sci.* 24 (2023) 9897, <https://doi.org/10.3390/IJMS24129897>.
- [46] J.C. Chachques, C. Gardin, N. Lila, L. Ferroni, V. Migonney, C. Falentin-Daudre, F. Zanotti, M. Trentini, G. Brunello, T. Rocca, V. Gasbarro, B. Zavan, Elastomeric cardiowrap scaffolds functionalized with mesenchymal stem cells-derived exosomes induce a positive modulation in the inflammatory and wound healing response of mesenchymal stem cell and macrophage, *Biomedicines* 9 (2021), <https://doi.org/10.3390/BIOMEDICINES9070824>.
- [47] D. Su, S. Swearson, T. Krongbaramee, H. Sun, L. Hong, B.A. Amendt, Exploring microRNAs in craniofacial regenerative medicine, *Biochem. Soc. Trans.* 51 (2023) 841–854, <https://doi.org/10.1042/BST20221448>.
- [48] C. Mangano, F.G. Mangano, J.A. Shibli, L.A. Roth, G. D' Addazio, A. Piattelli, G. Iezzi, Immunohistochemical evaluation of peri-implant soft tissues around machined and direct metal laser sintered (DMLS) healing abutments in humans, *Int. J. Environ. Res. Public Health* 15 (2018), <https://doi.org/10.3390/IJERPH15081611>.
- [49] F. Mangano, M. Bazzoli, L. Tettamanti, D. Farronato, M. Maineri, A. Macchi, C. Mangano, Custom-made, selective laser sintering (SLS) blade implants as a non-conventional solution for the prosthetic rehabilitation of extremely atrophied posterior mandible, *Lasers Med. Sci.* 28 (2013) 1241–1247, <https://doi.org/10.1007/S10103-012-1205-1>.